

Using Guest-Host Interactions to Optimise the Efficiency of TADF OLEDs

Paloma L. dos Santos,^a Jonathan S. Ward,^b Martin R. Bryce^b and Andrew P. Monkman^{a*}

a- OEM Research Group, Physics Department, Durham University, South Road, Durham
DH1 3LE, UK

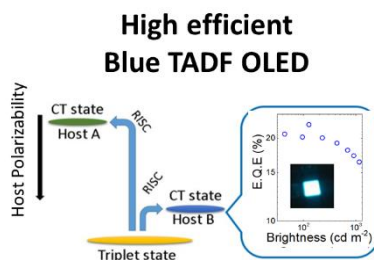
b- Department of Chemistry, Durham University, South Road, Durham DH1 3LE, UK

Corresponding Author

* Andrew P. Monkman (a.p.monkman@durham.ac.uk)

We show that the emitter *and* host combination must be optimized to minimize the reverse intersystem crossing (rISC) barrier and maximize thermally activated delayed fluorescence (TADF). The blue TADF emitter, 2,7-bis(9,9-dimethyl-acridin-10-yl)-9,9-dimethylthioxanthene-S,S-dioxide (DDMA-TXO2), has strong TADF character due to efficient charge transfer state (CT) formation. By combining DDMA-TXO2 with a host of the correct polarity (DPEPO) that relaxes the CT manifolds energy to become resonant with the lowest energy local triplet state of DDMA-TXO2, the emitter and host combination produce a minimum rISC barrier (ΔE_{ST}), which maximises TADF efficiency. We show that the sensitivity of these splittings is highly dependent on emitter environment and must be carefully tuned to optimised device performance. Devices utilising DDMA-TXO2 in DPEPO host show blue EL, CIE (0.16, 0.24) with maximum external quantum efficiency of 22.4 %. This high device performance is a direct consequence of optimising the TADF efficiency by this ‘host tuning’.

TOC GRAPHICS



KEYWORDS Blue OLED, TADF mechanism, Charge transfer state, Guest-Host interactions

Organic light-emitting diodes (OLEDs) are attracting great interest for display and lighting applications.^{1,2} Recently, a new emission mechanism was discovered, thermally activated delayed fluorescence (TADF) and since then, a huge improvement in the efficiency and brightness of fluorescent OLEDs has been observed.^{3,4}

Emission *via* the TADF mechanism uses thermal energy to vibronically couple the localised (³LE) and charge transfer (³CT) triplet states to mediate spin orbit coupling (SOC) to up-convert lower energy triplet excitons, which are in general not emissive at room temperature in organic molecules, into emissive singlet states of higher energy, thereby surpassing the imposed 25% internal quantum efficiency.⁴⁻⁹ One way to improve the TADF emission contribution is to minimize the energy splitting (ΔE_{ST}) between singlet and triplet states. Recent experimental studies¹⁰⁻¹² along with initial theoretical work¹³⁻¹⁵ identify that the SOC mechanism in these TADF systems is a complex second order process requiring vibronic coupling between ³CT and ³LE to mediate the spin flip back to the ¹CT state, the ³LE state mediates the SOC between the singlet and triplet CT states¹⁵. Hence whereas the CT states are very sensitive to the local environment¹⁰ the local triplet states are not, therefore the host differential effects the energy gaps which directly changes the rate of reverse intersystem crossing (rISC). So, to achieve very small ΔE_{ST} between each state the effect of the host environment must be taken into account and tuned to optimise device efficiency.

Here, we demonstrate how sensitive this ‘host tuning’ is and how when optimised yields extremely efficient devices. This study was made by analyses of the photophysical properties of 2,7-bis(9,9-dimethyl-acridin-10-yl)-9,9-dimethylthioxanthene-*S,S*-dioxide (DDMA-TXO2) in different hosts along with the photophysical properties of the acceptor and donor units separately. DDMA-TXO2 shows strong TADF character and blue emission. An efficient blue

OLED was fabricated in DPEPO host showing maximum E.Q.E. of 22.4 % at 127 cd/m² luminance, high brightness levels (>2,500 cd/m²), excellent resistance to roll-off up to 10 mA/cm² and low turn on voltage \approx 3 V. Moreover, we also observe CT relaxation dynamics, and from analyses of this we determine the correct CT energy that needs to be used to calculate the correct ΔE_{ST} .

In demonstrating how important it is to understand and take into consideration the effects of environment and relaxation on the energetics of the CT state, as in these D-A-D molecules the rate of rISC depends exponentially on the magnitude of the energy barrier, it is clear that small energy changes in the ΔE_{ST} , has a very profound effect on the rISC rate.

Figure 1 shows the normalized optical absorption (dash lines) and emission (full lines) spectra of the acceptor (A) and donor (D) units as well as the DDMA-TXO2 molecule. The donor unit is diluted in toluene solvent, the acceptor unit in methylcyclohexane (MCH) solvent and the D-A-D in both solvents. The chemical structure of DDMA-TXO2 is also shown in **Figure 1**. The synthesis and chemical characterization are given in **Figure S1**. The absorption spectrum of D-A-D shows two peaks. The peak around 290 nm is the same as that observed in the donor unit spectrum; however, the second peak, around 360 nm, does not appear in either the D or the A absorption spectra. We assigned this peak to the ‘direct’ CT absorption, an $n-\pi^*$ (or mixed $\pi\pi^*/n\pi^*$) transition in the D-A-D molecule.¹² The D-A-D emission spectra show clear and strong CT emission evidenced by its Gaussian band shape and red shift compared to the individual **D** and **A** emission spectra. The PL spectra move to longer wavelength with increasing solvent polarity, showing a strong positive solvatochromism, as observed before in other D-A-D type molecules.^{4,16,17}

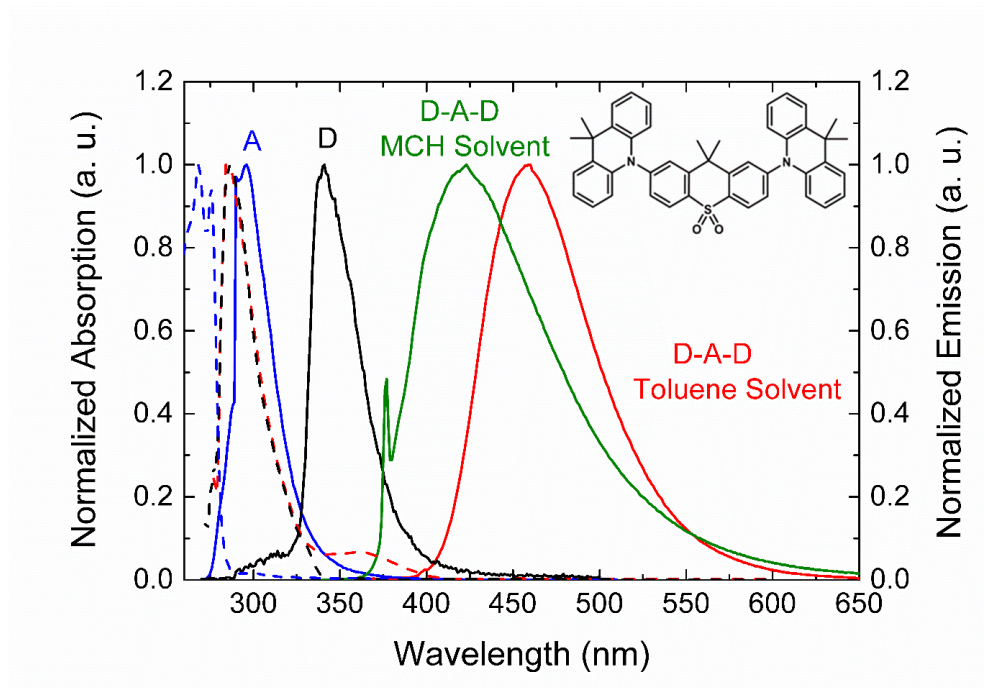


Figure 1. Normalized absorption and emission spectra of acceptor (A), donor (D), and D-A-D (DDMA-TXO₂) molecules. Donor unit is diluted in toluene solvent, acceptor unit in MCH solvent and D-A-D in both solvents. The acceptor and donor units were excited at 266 nm and the D-A-D at 337 nm. Inset graph shows the chemical structure of DDMA-TXO₂.

The contribution of emissive states that at some point in their lifetime have resided in a triplet excited state, to the total emission was determined by comparing the emission intensity in aerated and degassed toluene solutions (**Figure S2**). Upon removing oxygen, the intensity increases by a factor of 3.70, indicating that the contribution of DF to the overall emission is 78%. Also, it is shown that the emission spectra obtained in degassed and aerated solutions match each other, showing that delayed fluorescence (DF) and prompt fluorescence arise from the same ¹CT state. Due to the high DF contribution, we proceeded to investigate the DF mechanism in solid state, which can confirm DDMA-TXO₂ is a promising blue emitter for OLED applications.

Figure 2 shows the time dependent emission decay curves at various temperatures of DDMA-TXO2 in zeonex matrix from the early prompt emission (Time delay (TD) = 1.1 ns) to the end of the DF (TD = 89 ms). The curves were obtained with 355 nm excitation (>200 μ J) giving direct CT photo creation. The decay curves at higher temperatures show clear double exponential decays, assigned as prompt and delayed emission regions (of the same species, having an effective longer life time due to rate of slow rISC). The DF emission has clearly higher intensity at high temperatures, indicative of a TADF contribution. At low temperatures, the curves show prompt emission, followed by an interval during which any emission was below the detection noise floor of the iCCD, and then, at longer time delays, phosphorescence emission appears. The emission at very long time delays, shows higher intensity at low temperatures, as expected for triplet emission.

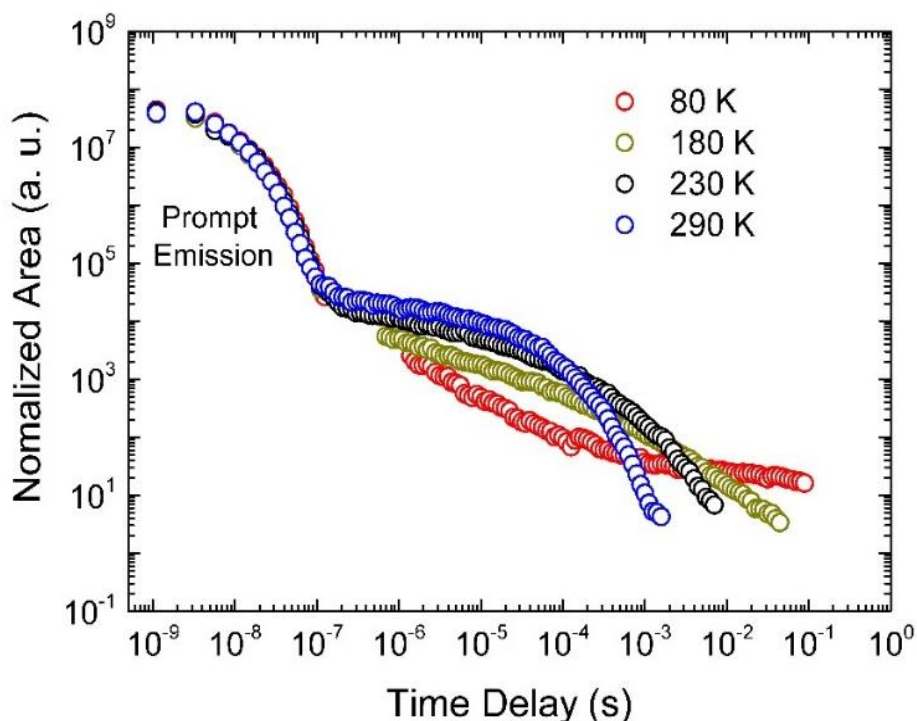


Figure 2. Time resolved fluorescence decay of DDMA-TXO2 in zeonex matrix.

Figure 3 shows the analyses of the normalized spectra in the entire region of study at 80 K (a) and 290 K (b). At 80 K, from TD=1.1 to TD = 124 ns, the transition ${}^1\text{CT} \rightarrow \text{S}_0$ is observed, and has onset at (3.17 ± 0.02) eV. At longer time delays, a very weak emission is observed, having negligible intensity. From TD=1.3 μs to TD = 90 ms, a red shifted emission is observed, onset at (3.02 ± 0.02) eV which is assigned as phosphorescence emission (PH). The PH spectrum detected in the DDMA-TXO2 molecules was compared with the PH spectra of the individual donor and acceptor units (**Figure S3**). Most likely, the DDMA-TXO2 triplet level is a mix of both localised triplet (${}^3\text{LE}$) states of the donor and acceptor unit, as seen in other similar D-A-D TADF molecules.¹¹ Therefore, the energy splitting between ${}^1\text{CT}$ and ${}^3\text{LE}$ was found to be $\Delta E_{ST} = (0.15 \pm 0.03)$ eV. At 290 K, the emission spectra of DDMA-TXO2 showed a different behaviour. In the entire region of analyses, from TD = 1 ns to TD = 1.4 ms, only the transition ${}^1\text{CT} \rightarrow \text{S}_0$ is observed with onset at (3.17 ± 0.02) eV. This can be explained by the fact that at high temperature, the rISC process is favourable and delayed fluorescence is efficiently observed. At low temperatures, triplet states do not have enough thermal energy to cross the activation barrier to the ${}^1\text{CT}$ manifold and PH is favoured over the rISC process. Furthermore, we analysed the intensity dependence of the DF emission (TD = 500 ns, Ti= 1500 ns) as a function of the laser excitation dose, and a linear gradient of 0.97 ± 0.01 was found (**Figure S4**). This result confirms beyond doubt the thermally assisted mechanism as opposed to triplet-triplet annihilation (TTA) as the origin of emission. Generally, TADF complexes show slope close to 1 at low and high excitation doses while TTA complexes show slope close to 2 at low excitation doses turning to slope close to 1 at high excitation doses.¹⁸

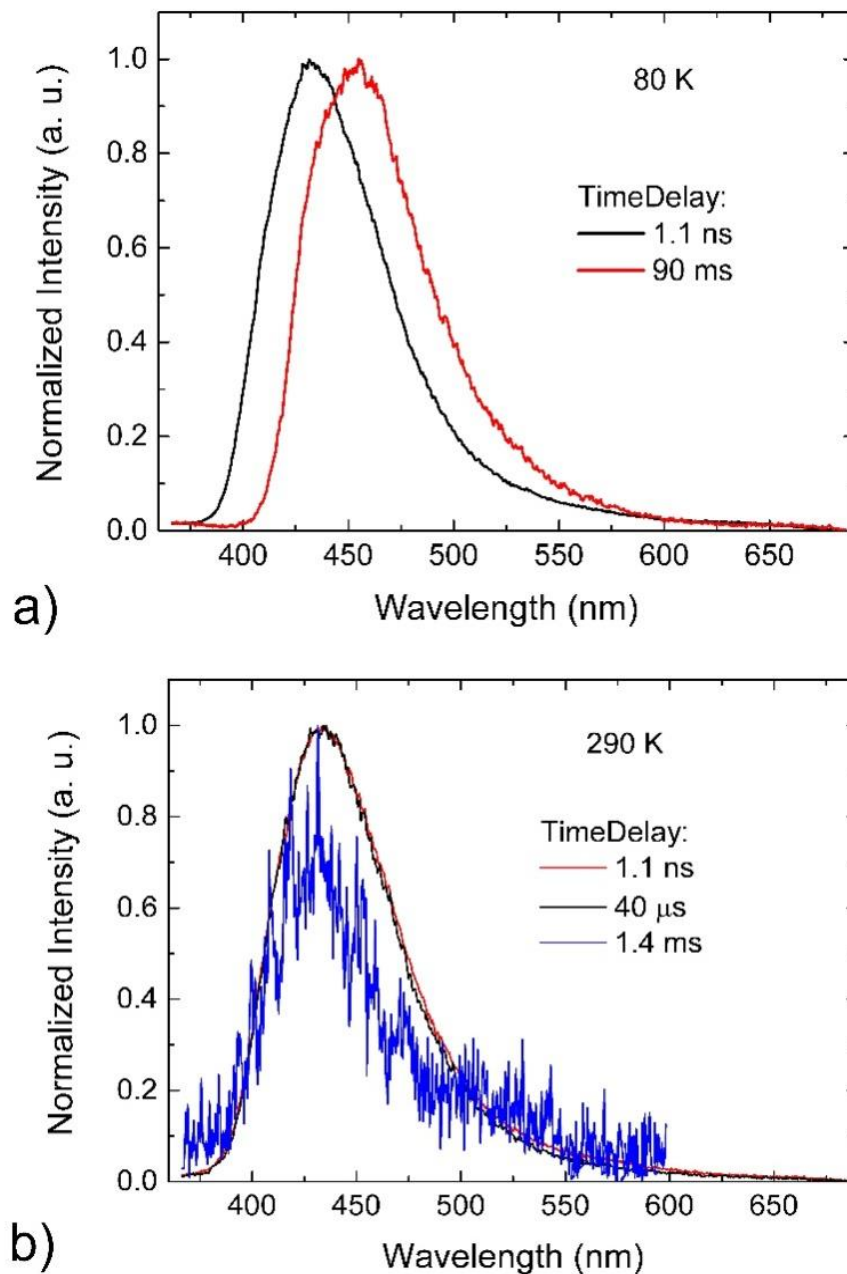


Figure 3. Time resolved normalized emission spectra of DDMA-TXO2 in zeonex matrix at a) 80 K and b) 290 K.

After showing the strong TADF mechanism of DDMA-TXO2 in zeonex matrix, we proceed to investigate how the mechanism depends on the polarity of the medium in which the emitter is dispersed. Bis[2-(di-(phenyl)phosphino)-phenyl]ether oxide (DPEPO) was chosen as a

potential host for DDMA-TXO2 as it has a triplet level comparable to DDMA-TXO2. The PH onset of DPEPO was found to be at (3.05 ± 0.02) eV (**Figure S5**), which is close to, but energetically above, the PH onset of DDMA-TXO2 in zeonex matrix, (3.02 ± 0.02) eV.

Figure 4 shows the time dependent emission decay curves at various temperatures of DDMA-TXO2 in DPEPO matrix from the early prompt emission (TD = 1.1 ns) to the end of the DF (TD = 89 ms). The curves were obtained with 355 nm excitation ($>200 \mu\text{J}$). The decay curves at higher temperatures show clear double exponential decays, assigned as prompt and delayed emission regions (of the same species). At the beginning of the DF emission, the curves show clearly higher intensity at high temperatures, indicative of a TADF contribution. However, after $\sim 44 \mu\text{s}$ (see **Figure 4**) the temperature behaviour changes and the emission drops as the system temperature increases. The later temperature behaviour is unexpected for a TADF mechanism, and it will be explained later by analyses of ^1CT energy levels at 80 and 290 K.

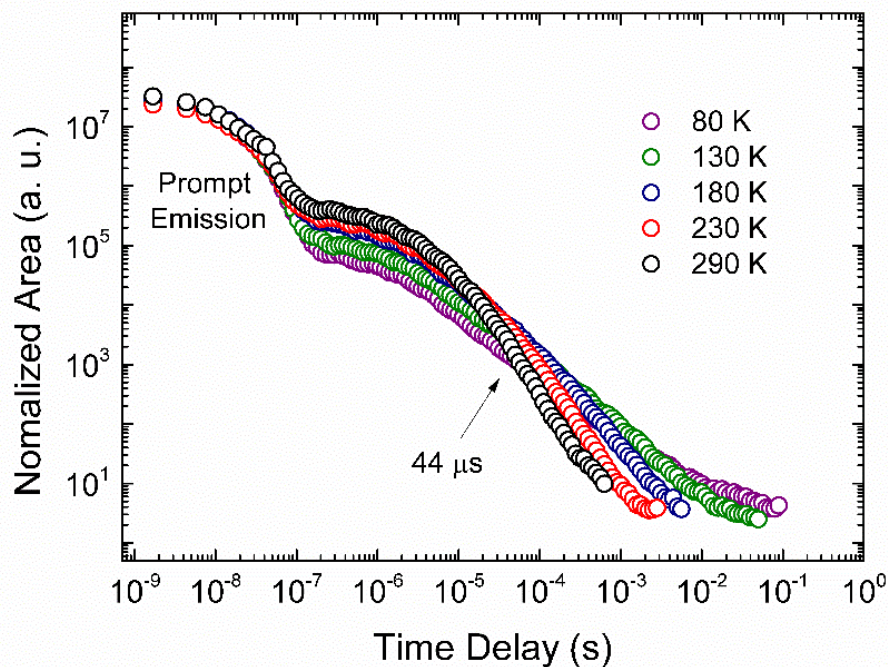


Figure 4. Time resolved fluorescence decay of DDMA-TXO2 in DPEPO matrix.

Figure 5 shows the analyses of the normalized spectra in the entire region of study at 80 K (a) and 290 K (b). At 80 K, during the prompt emission, a continuous dynamic redshift is observed from TD = 1.1 to TD = 120.7 ns. This red shift is associated with the energetic relaxation of the CT state, which stabilizes after TD = 120.7 ns. The spectra have onset at (3.08 ± 0.02) eV and (2.93 ± 0.02) eV for TD = 1.1 ns and TD = 120.7 ns, respectively. After this time the spectra show no further shift until TD = 50 ms. Thus, only the transition ${}^1\text{CT} \rightarrow \text{S}_0$ is observed in DDMA-TXO2:DPEPO at 80 K. At 290 K, the continuous redshift with increasing time delay is also observed during the prompt fluorescence region. However, at high temperatures the prompt emission region is shorter, and the stabilization of ${}^1\text{CT}$ occurs after TD = 68.5 ns. The spectra have onset at (3.03 ± 0.02) eV and (2.95 ± 0.02) eV for TD = 1.1 ns and TD = 68.5 ns respectively. After this time no further relaxation is observed until TD = 0.2 ms. Furthermore, the intensity dependence of the DF emission (TD = 500 ns, Ti = 5000 ns) was analysed as a function of the laser excitation dose, and a linear gradient of 0.94 ± 0.01 was found (**Figure S6**), confirming the thermally assisted mechanism.

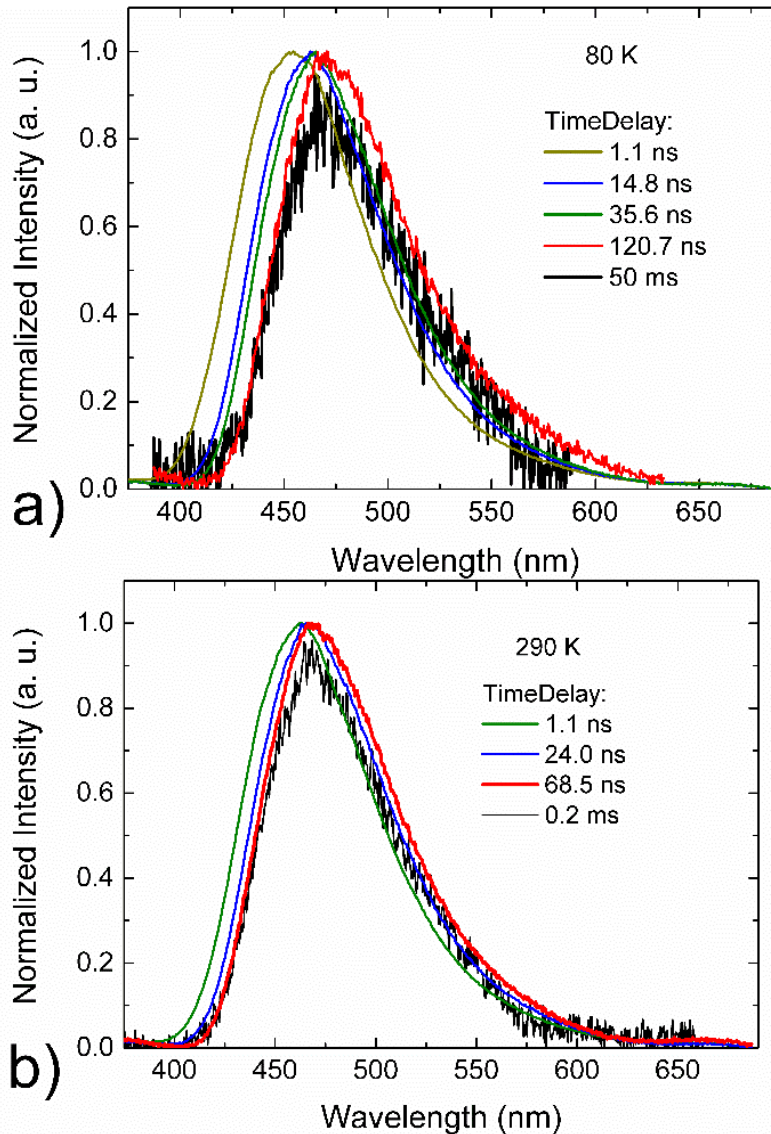


Figure 5. Time resolved normalized emission spectra of DDMA-TXO2 in DPEPO matrix at a) 80 K and b) 290 K.

Considering that the localised excitonic triplet states, ^3LE , will be unaffected by the polarity of the host environment, the triplet levels of DDMA-TXO2 in DPEPO should also have onset at (3.02 ± 0.02) eV (**Figure 3.a**). Therefore, to evaluate the ΔE_{ST} barrier for rISC, we must take into consideration this observed dynamic relaxation of the CT state. We must take the magnitude of the unrelaxed ^1CT energy level (in DPEPO) because the relaxation of the CT state only begins after the CT state has formed, *i.e.* the energy of the ^1CT state transferred to from the

³LE triplet state during rISC. Consequently, the energy splitting between ¹CT and ³LE states at 80 and 290 K are $\Delta E_{ST} = (0.06 \pm 0.03)$ eV and $\Delta E_{ST} = (0.01 \pm 0.03)$ eV, respectively in DPEPO host. Also, comparing the energy of the ¹CT state in zeonex and DPEPO there is a static red shift of the CT state (seen at 1 ns) of ca. 140 meV because of the higher polarity of the DPEPO host matrix. It is very important to understand and take into consideration these effects of environment and relaxation on the energetics of the CT state, as in these D-A-D molecules the rate of rISC depends exponentially on the magnitude of the energy barrier, thus decreasing this from 0.15 eV to 0.01 eV has a very profound effect on the rISC rate and even changing from 0.06 eV to 0.01 eV will cause significant changes to the rISC rate, especially at low temperatures. So to correctly obtain the ¹CT energy *for the reverse crossing step*, it must be measured at the earliest possible time after creation and not from the long time (μ s) CT emission. Hence, at 290 K the ΔE_{ST} of DDMA-TXO2 is very small in magnitude and the rISC process is thus fast, leading to a more rapidly decaying DF component. On the other hand, at 80 K, the ΔE_{ST} is larger, and the rISC process is slower, leading to a longer lived DF component. This explains the unexpected temperature behaviour of the DF after TD = 44 μ s (**Figure 4**). This analysis also explains why the prompt emission is faster at 290 K, because at this temperature, the rISC has a higher rate, decreasing the time over which ‘pure’ prompt emission is observed. Moreover, it is also observed that as ΔE_{ST} is so small, rISC is maximized and the transition ³LE \rightarrow S₀ is not observed in DPEPO host because all triplets are harvested by rISC which strongly out competes phosphorescence decay.

Therefore, it is clear that for DDMA-TXO2 in DPEPO host, the initial ¹CT state energy lies very close to the triplet states, as compared to in zeonex host, yielding a very small ΔE_{ST} , and consequently, high efficient TADF mechanism.

The photoluminescence quantum yields (PLQY) also show strong consequences of the ΔE_{ST} values in different environments. DDMA-TXO2 in zeonex matrix shows PLQY values of (30 \pm 3) % in nitrogen atmosphere and (18 \pm 3) % in air. Whereas, the film in DPEPO matrix shows PLQY values of (95 \pm 3) % in nitrogen atmosphere and (92 \pm 3) % in air. The later values are much higher than those found in zeonex matrix because the high-lying CT states yields a slow rISC rate (by at least an order of magnitude ¹⁵). Thus the residence time in the low lying ³LE state decays by non-radiative processes in direct competition with rISC, leading to a lower PLQY values. However, in DPEPO matrix, the ΔE_{ST} is much smaller and an efficient repopulation of ¹CT state via rISC process occurs, leading to very high PLQY values. These results clearly show how a solid host still plays a major role in optimising the TADF efficiency and provides a unique way to tune the efficiency of an OLED.

To evaluate the potential of DDMA-TXO2:DPEPO in OLEDs, devices were fabricated. The architecture of the optimized device was: ITO/ NPB(40nm)/ TCBPA(10nm)/ 13%DDMA-TXO2:DPEPO(30nm)/ DPEPO(10)/ TPBi(40nm)/ LiF/ Al (**Figure 6**). NPB is *N,N'*-bis(naphthalene-1-yl)-*N,N'*-bis(phenyl)-benzidine, TCBPA is 4,4-(diphenylmethylene)bis(*N,N*-diphenylaniline) and TPBi is 1,3,5-tris(*N*-phenylbenzimidazol-2-yl)benzene. The devices show blue emission, with the peak of the electroluminescence spectra (EL) at 465 nm (**Figure 6**). However, the pure emission was achieved only after including the thin single undoped DPEPO layer in the structure of the device. Devices without this extra layer showed an extra peak at 625 nm assigned to exciplex formation between the emissive layer DDMA-TXO2 and the transport layer TPBi (**Figure S7**).

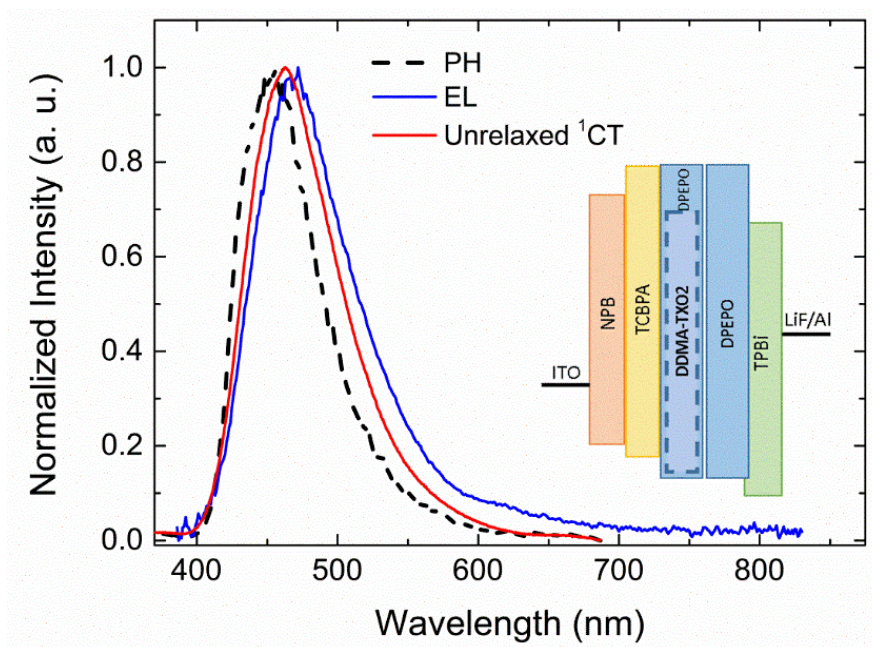


Figure 6. Phosphorescence (PH), electroluminescence (EL) and unrelaxed ^1CT spectra. Inset figure architecture of the optimized DDMA-TXO2:DPEPO device.

Devices as described in **Figure 6** show a maximum external quantum efficiency (E.Q.E.) of 22.4% at 127 cd/m^2 with commission internationale de l'éclairage (CIE) chromaticity coordinates of (0.16, 0.24), peak emission wavelength 465 nm and luminous efficiency of 17.2 lm/W , all devices tested with this structure show an initially increase in efficiency of about 10%, before stabilizing. The device also shows good E.Q.E. value, 17.3 %, at high brightness, 913 cd/m^2 . **Figure 7** shows the E.Q.E. *versus* current density, brightness *versus* current density, current density *versus* bias curves and E.Q.E. *versus* brightness curves. The device shows good E.Q.E. values, high brightness levels $>2,500 \text{ cd/m}^2$, excellent resistance to roll-off up to 10 mA/cm^2 and low turn on voltage $\sim 3 \text{ V}$. The excellent performance is due to a very small energy splitting between ^1CT and the localised triplet states (^3LE) as confirmed by the photophysical analyses. These very promising device results clearly show that the host tuning to maximise TADF efficiency directly translates in enhances OLED performance.

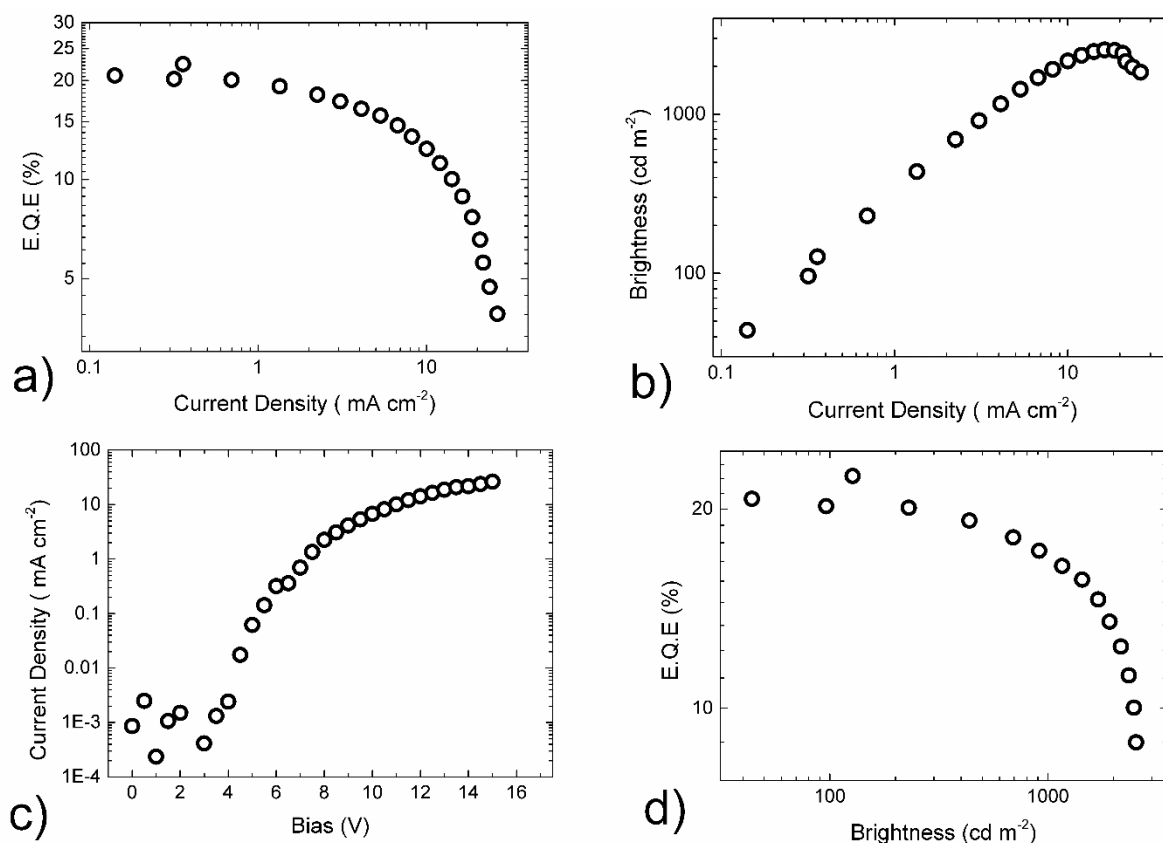


Figure 7. a) E.Q.E. *versus* current density b) brightness *versus* current density c) current density *versus* bias and d) E.Q.E. *versus* brightness curves for DDMA-TXO2:DPEPO devices.

Figure 6 also shows the PH spectra of DDMA-TXO2 in zeonex matrix and the unrelaxed ¹CT state in DPEPO host, for comparison. As can be seen, the onset of the unrelaxed ¹CT and EL are isoenergetic, supporting the proposal that the unrelaxed energy of the CT state is the energy ‘seen’ at the rISC step. The onset of both, EL and PH spectra are almost isoenergetic, yielding highly efficient TADF and hence efficient devices. The small peak shift of the EL compared to the PL is due to a residual exciplex contribution on the red side of the EL band.

In summary, we report the photophysical properties of an efficient blue TADF emitter molecule, DDMA-TXO2, along with the photophysics of its constituent donor and acceptor units. DDMA-TXO2 shows a strong and clear CT state in solution and solid state. The TADF mechanism was readily identified in solid state in different hosts. An in-depth photophysical study reveals the ^1CT state is lowered in energy within the polar host DPEPO, relaxed through the high polarity of the DPEPO compared to non-polar host materials, and becomes very close in energy to the triplet states of DDMA-TXO2, which are unaffected by the host environment, giving rise to a very small $\Delta E_{ST} = (0.01 \pm 0.03)$ eV. This host tuning effect optimises the rISC rate as seen in the DF decay kinetics giving rise to efficient blue emission, shows the need to optimize how the host polarisability perturbs the emitter in the correct way to minimize the rISC barrier and maximize TADF contribution. This enhanced TADF efficiency directly translates into device performance. Devices utilising DPEPO host show a maximum external quantum efficiency of 22.43 % at 127.4 cd/m^2 luminance, high brightness levels $>2,500 \text{ cd/m}^2$, excellent resistance to roll-off up to 10 mA/cm^2 and low turn on voltage ~ 3 V. It is clear that both the emitter and host combination must be designed and optimised together to produce a minimum rISC barrier in order to achieve highly efficient TADF OLEDs. It is also seen how sensitive the rISC rate is to the host and how carefully this tuning needs to be made. We further observe that in the polar DPEPO host the CT state relaxes dynamically, over the first 100 ns, however when calculating the correct energy gap for the rISC step one must use the unrelaxed (earliest time) energy of the CT state to correctly estimate the $^1\text{CT } ^3\text{LE}$ gap ‘seen’ at the rISC step. These results represent an important step forward in the understanding of new emitter-host combinations to achieve enhanced efficiency TADF-OLEDs and these design principles should be readily applicable to a wide range of new TADF-OLED systems.

Experimental Methods

The synthesis and characterization data for 2,7-bis(9,9-dimethyl-acridin-10-yl)-9,9-dimethylthioxanthene-*S,S*-dioxide (DDMA-TXO2) are given in detail in the **S1**.

Three types of samples were studied in this work: solutions in toluene and in methylcyclohexane (MCH) solvents (10^{-3} to 10^{-5} M), films produced in zeonex matrix (organic material 2.5 mg/mL :zeonex 180 mg/mL 1:1 v/v) and thin film produced in DPEPO host (11% DDMA-TXO2:DPEPO). The solutions were stirred for 24 hours and they were also degassed to remove all the oxygen dissolved in the solutions by 4 freeze-thaw cycles to measure the effect of oxygen quenching. Films in zeonex matrix were fabricated by spin-coating on quartz substrates at 500 rpm during 60 seconds. Thin film in a DPEPO host was made by co-evaporation deposition onto transparent sapphire substrates using a Kurt J. Lesker Spectros II deposition system under vacuum, 10^{-6} mbar, at a steady evaporation rate of $\sim 2.3 \text{ \AA/s}$ and $\sim 0.28 \text{ \AA/s}$ for host and guest materials, respectively.

Steady state absorption and emission spectra were acquired using a UV-3600 Shimadzu spectrophotometer and a JobinYvon Horiba Fluoromax 3, respectively. Time resolved spectra were obtained by exciting the sample with a Nd:YAG laser (EKSPLA), 10 Hz, 355 nm/266 nm or by using a Nitrogen laser, 10 Hz, 337 nm. For Nd:YAG laser and Nitrogen laser the earliest emission available for collection were at time delay (TD) at 1 ns and 30 ns, respectively. Sample emission was directed onto a spectrograph and gated iCCD camera (Stanford Computer Optics). Photoluminescence quantum yields (PLQY) were acquired using PLQY Quantaaurus – QY

Hamamatsu. The PLQY values were calculated from the average of 7 values obtained with excitation between 280 and 340 nm (10 nm step).

OLED devices were fabricated using pre-cleaned indium-tin-oxide (ITO) coated glass substrates purchased from Ossila with a sheet resistance of $20 \Omega/\text{cm}^2$ and ITO thickness of 100 nm. The OLED devices had a pixel size of 4 mm by 4 mm. The small molecule and cathode layers were thermally evaporated using the Kurt J. LeskerSpectros II deposition chamber at 10^{-6} mbar.

ASSOCIATED CONTENT

Supporting Information available: Synthetic details, additional photophysical and OLED data.

AUTHOR INFORMATION

P. L. dos Santos and J. S. Ward contributed equally to the experimental work.

ACKNOWLEDGMENT

P. L. dos Santos thanks CAPES Foundation, Ministry of Education of Brazil, Brasilia - DF 70040 - 020, Brazil, in particular the Science Without Borders Program for a PhD studentship, Proc. 12027/13-8. J. S. Ward thanks EPSRC for funding. All authors thank EPSRC grant EP/L02621X/1. We also thank Hamamatsu for providing the PLQY equipment (Quantaaurus – QY).

REFERENCES

- (1) Tang, C. W.; VanSlyke, S. A. Organic Electroluminescent Diodes. *Appl. Phys. Lett.* **1987**, *51*, 913–915.
- (2) Reineke, S.; Lindner, F.; Schwartz, G.; Seidler, N.; Walzer, K.; Lüssem, B.; Leo, K. White

- Organic Light-Emitting Diodes with Fluorescent Tube Efficiency. *Nature* **2009**, *459*, 234–238.
- (3) Goushi, K.; Yoshida, K.; Sato, K.; Adachi, C. Organic Light-Emitting Diodes Employing Efficient Reverse Intersystem Crossing for Triplet-to-Singlet State Conversion. *Nat. Photonics* **2012**, *6*, 253–258.
- (4) Dias, F. B.; Bourdakos, K. N.; Jankus, V.; Moss, K. C.; Kamtekar, K. T.; Bhalla, V.; Santos, J.; Bryce, M. R.; Monkman, A. P. Triplet Harvesting with 100% Efficiency by Way of Thermally Activated Delayed Fluorescence in Charge Transfer OLED Emitters. *Adv. Mater.* **2013**, *25*, 3707–3714.
- (5) Higuchi, T.; Nakanotani, H.; Adachi, C. High-Efficiency White Organic Light-Emitting Diodes Based on a Blue Thermally Activated Delayed Fluorescent Emitter Combined with Green and Red Fluorescent Emitters. *Adv. Mater.* **2015**, *27*, 2019–2023.
- (6) Jankus, V.; Data, P.; Graves, D.; McGuinness, C.; Santos, J.; Bryce, M. R.; Dias, F. B.; Monkman, A. P. Highly Efficient TADF OLEDs: How the Emitter-Host Interaction Controls Both the Excited State Species and Electrical Properties of the Devices to Achieve Near 100% Triplet Harvesting and High Efficiency. *Adv. Funct. Mater.* **2014**, *24*, 6178–6186.
- (7) Uoyama, H.; Goushi, K.; Shizu, K.; Nomura, H.; Adachi, C. Highly Efficient Organic Light-Emitting Diodes from Delayed Fluorescence. *Nature* **2012**, *492*, 234–238.
- (8) Zhang, Q.; Li, B.; Huang, S.; Nomura, H.; Tanaka, H.; Adachi, C. Efficient Blue Organic Light-Emitting Diodes Employing Thermally Activated Delayed Fluorescence. *Nat. Photonics* **2014**, *8*, 1–7.
- (9) Wang, H.; Xie, L.; Peng, Q.; Meng, L.; Wang, Y.; Yi, Y.; Wang, P. Novel Thermally

- Activated Delayed Fluorescence Materials-Thioxanthone Derivatives and Their Applications for Highly Efficient OLEDs. *Adv. Mater.* **2014**, *26*, 5198–5204.
- (10) Santos, P. L.; Ward, J. S.; Data, P.; Batsanov, A. S.; Bryce, M. R.; Dias, F. B.; Monkman, A. P. Engineering the Singlet–triplet Energy Splitting in a TADF Molecule. *J. Mater. Chem. C* **2016**, *4*, 3815-3824.
- (11) Nobuyasu, R. S.; Ren, Z.; Griffiths, G. C.; Batsanov, A. S.; Data, P.; Yan, S.; Monkman, A. P.; Bryce, M. R.; Dias, F. B. Rational Design of TADF Polymers Using a Donor-Acceptor Monomer with Enhanced TADF Efficiency Induced by the Energy Alignment of Charge Transfer and Local Triplet Excited States. *Adv. Opt. Mater.* **2015**, DOI: 10.1002/adom.201500689.
- (12) Dias, F. B.; Santos, J.; Graves, D.; Data, P.; Nobuyasu, R. S.; Fox, M. A.; Batsanov, A. S.; Palmeira, T.; Bryce, M. R.; Monkman, A. P.; The Role of Local Triplet Excited States in Thermally-Activated Delayed Fluorescence: Photophysics and Devices. *Adv. Science*, **2016**, DOI: 10.1002/advs.201600080.
- (13) Lim, B. T.; Okajima, S.; Chandra, A. K.; Lim, E. C. Radiationless Transitions in Electron Donor-Acceptor Complexes: Selection Rules for $S_1 \rightarrow T$ Intersystem Crossing and Efficiency of $S_1 \rightarrow S_0$ Internal Conversion. *Chem. Phys. Lett.* **1981**, *79* (1), 22–27.
- (14) Marian, C. M. On the Mechanism of the Triplet-to-Singlet Upconversion in the Assistant Dopant ACRXTN. *J. Phys. Chem. C* **2016**, *120*, 3715–3721.
- (15) Gibson, J.; Monkman, A. P.; Penfold, T.; The Importance of Vibronic Coupling for Efficient Reverse Intersystem Crossing. *ChemPhysChem* DOI: 10.1002/cphc.201600662.
- (16) Dias, F. B.; Pollock, S.; Hedley, G.; Pålsson, L.; Monkman, A.; Perepichka, I. I.; Perepichka, I. F.; Tavasli, M.; Bryce, M. R. Intramolecular Charge Transfer Assisted by

- Conformational Changes in the Excited State. *J. Phys. Chem. B* **2006**, *110*, 19329–19339.
- (17) Youn Lee, S.; Yasuda, T.; Nomura, H.; Adachi, C. High-Efficiency Organic Light-Emitting Diodes Utilizing Thermally Activated Delayed Fluorescence from Triazine-Based Donor-Acceptor Hybrid Molecules. *Appl. Phys. Lett.* **2012**, *101*, 1–5.
- (18) Dias, F. B. Kinetics of Thermal-Assisted Delayed Fluorescence in Blue Organic Emitters with Large Singlet – Triplet Energy Gap Subject Areas : Author for Correspondence : *R. Soc.* **2015**, *373*, 20140447.